Nanotechnology **32** (2021) 045201 (9pp) https://doi.org/10.1088/1361-6528/abbf6a

Chemistry of ruthenium as an electrode for metal–insulator–metal capacitor application

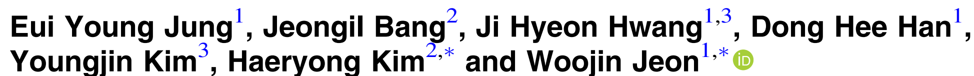

Eui Young Jung[1], Jeongil Bang[2], Ji Hyeon Hwang[1,3], Dong Hee Han[1], Youngjin Kim[3], Haeryong Kim[2,*] and Woojin Jeon[1,*]

[1] Department of Advanced Materials Engineering for Information and Electronics, Kyung Hee University, Yongin, Gyeonggi 17104, Republic of Korea
[2] Inorganic Material Laboratory, Device and System Research Center, Samsung Advanced Institute of Technology, Suwon, Gyeonggi 16678, Republic of Korea
[3] Soft Hybrid Materials Research Center, Korea Institute of Science and Technology, Seoul 02792, Republic of Korea

E-mail: hryong.kim@samsung.com and woojin.jeon@khu.ac.kr

Received 9 September 2020, revised 1 October 2020
Accepted for publication 8 October 2020
Published 28 October 2020

Abstract

Notwithstanding its excellent properties such as high work function and low resistance, Ru has not been widely applied in the preparation of electrodes for various electronic devices. This is because of the occurrence of severe morphological degradation in the actual devices employing Ru. Herein, we investigated Ru chemistry for electrode application and the degradation mechanism of Ru during subsequent processes such as thin film deposition or thermal annealing. We revealed that subsurface oxygen induces Ru degradation owing to the alteration of Ru chemistry by the pretreatment under various gas ambient conditions and due to the growth behavior of TiO_2 deposited via atomic layer deposition (ALD). The degradation of Ru is successfully ameliorated by conducting an appropriate pretreatment prior to ALD. The TiO_2 thin film deposited on the pretreated Ru electrode exhibited a rutile-phased crystal structure and smooth surface morphology, thereby resulting in excellent electrical properties. This paper presents an important development in the application of Ru as the electrode that can facilitate the development of various next-generation electronic devices.

Supplementary material for this article is available online

Keywords: ruthenium, ruthenium oxide, subsurface oxygen, metal–insulator–metal capacitor, electrode, surface morphology, electrical property

(Some figures may appear in colour only in the online journal)

1. Introduction

In semiconductor devices, the metal–insulator–metal (MIM) systems have been widely employed as a selector, capacitor, or switching component [1–8]. Depending on the role of the MIM system, various methods to control its electrical properties, such as capacitance and leakage current, have been investigated [9–12]. Among them, the use of high dielectric constant (k) materials, such as Al_2O_3, ZrO_2, HfO_2, and TiO_2, as an insulator has been studied to increase the capacitance for MIM capacitors [13–16]. There are several requirements involved in employing the high-k materials as an MIM capacitor dielectric, such as a high dielectric constant and a low leakage current [14, 17]. Among the various high-k materials, the $ZrO_2/Al_2O_3/ZrO_2$ (ZAZ) structure [18–20] successfully satisfies these requirements; thus, it has been widely employed as an MIM capacitor dielectric for over a decade. However, the relatively lower k value of the ZAZ structure (<30) limits its further application for next-generation semiconductor devices with a design rule of <1x nm. Consequently, high-k materials, such as TiO_2 [21–25] and $SrTiO_3$ [26–31], have attracted considerable attention

[*] Authors to whom any correspondence should be addressed.

 © 2020 IOP Publishing Ltd Printed in the UK

however, they inherently exhibit a poor leakage current characteristics because of their small bandgap, which results in generally low band offsets with metal electrodes [16, 23]. Moreover, TiO_2 has several crystal structures, such as anatase, rutile, and brookite phases. Among them, the rutile phase is the most favorable structure because its k is ~100. However, it is difficult to acquire the rutile phase under low-temperature processing conditions [21, 32, 33]. Meanwhile, TiN has been employed as a metal electrode in various semiconductor devices. However, because of its relatively low work function of ~4.5 eV, it serves an ineffective electrode for devices based on higher-k materials as a low work function generally induces a small conduction band offset, thereby resulting in a high leakage current. Furthermore, the TiN electrode easily reduces an adjacent high-k dielectric, thus inducing the formation of various types of defects in high-k dielectrics [7, 34]. This undesirable TiN electrode reaction and presence of high-k dielectric might crucially aggravate the electrical properties of MIM capacitors.

To overcome these technical issues, Ru has been introduced as a promising electrode material for MIM capacitors with TiO_2-based high-k dielectrics [35–37]. Notably, Ru has a relatively higher work function of ~4.7 eV, and it can be further increased to ~5.1 eV when oxidized to RuO_2, which can also be utilized as an electrode because of its electrically conductive property and resistivity of ~46 $\mu\Omega \cdot$ cm [38–43]. In addition, Ru plays a crucial role toward obtaining the rutile phase of TiO_2 by deriving a certain epitaxial-like growth from a near-identical lattice parameter of RuO_2 and rutile-phased TiO_2 [35, 40]. Therefore, employing the Ru electrode is inevitable to demonstrate MIM capacitors for next-generation semiconductor devices by adapting the rutile-phased TiO_2 as the capacitor dielectric. However, other technical problems have ensued from the lower oxide formation energy of Ru than that of other dielectrics. Firstly, this comparatively minimal oxide formation energy of Ru induces the development of various oxides such as RuO_2, RuO_3, or RuO_4, which typically complicates the evaluation of the deposition process for the stable stoichiometric oxide of RuO_2 [43]. Moreover, the low redox resistance of Ru causes severe morphological degradation during subsequent oxide deposition processes [44]. Consequently, employing Ru as an electrode for MIM capacitors has been tentative; therefore, the utilization of the rutile-phased TiO_2 thin film for next-generation semiconductor applications has been hampered.

In this work, Ru chemistry is comprehensively investigated to verify the applicability of Ru as a metal electrode for MIM capacitors using a rutile-phased TiO_2 thin film. The mechanism of the morphological degradation of Ru during subsequent deposition processes is also established. Based on the revealed morphological degradation mechanism, the pretreatment process of the Ru electrode was investigated. Furthermore, the growth behavior and electrical properties of the TiO_2 thin film were evaluated. Finally, the MIM capacitor that consisted of Ru and TiO_2 as the electrode and insulator, respectively, was demonstrated for next-generation semiconductor applications.

2. Experimental procedure

Here, 30 nm thick Ru films were deposited onto 100 nm thick SiO_2/Si substrates via DC magnetron sputtering in an ultra-high vacuum setup. A thermal annealing process on the Ru substrates, called 'pretreatment', was performed prior to the TiO_2 thin film deposition by using a tube furnace at 300 °C for 30 m with varied gas ambient of 99.999% N_2, 95% N_2 + 5% H_2 ($N_2 + H_2$), and 95% N_2 + 5% O_2 ($N_2 + O_2$). Thereafter, the TiO_2 thin films were deposited via atomic layer deposition (ALD) using $Ti(OC_3H_7)_4$ (titanium tetra-isopropoxide, TTIP) and O_3 (200 g $\cdot$ m^{-3}) as the Ti precursor and oxygen source, respectively; the sequence consisted of TTIP feeding, Ar purge, O_3 feeding, and Ar purge steps of 0.5, 10, 1, and 10 s, respectively, at a growth temperature of 250 °C. The modified TiO_2 ALD sequences were also conducted under very similar processing conditions of time, thermal budget, and chamber pressure as that of the normal TiO_2 ALD; the Ti-precursor-only sequence, which consisted of TTIP feeding, Ar purge, Ar purge (instead of O_3), and Ar purge steps of 0.5, 10, 1, and 10 s, respectively, or the O_3-only sequence, which comprised Ar purge (instead of Ti precursor), Ar purge, O_3 feeding, and Ar purge steps of 0.5, 10, 1, and 10 s, respectively. To measure the electrical properties, an MIM capacitor was fabricated with a top electrode (TE), which consisted of a 30 nm thick RuO_2 and a 50 nm thick Pt film that were deposited via reactive and DC sputtering, respectively, defined by a metal shadow mask with a 300 mm diameter hole. After the TE deposition, post-metallization annealing was performed at 400 °C for 30 m under $N_2 + O_2$ ambient conditions.

The thickness of the TiO_2 films was determined by calculations from the layer density that was measured via x-ray fluorescence spectroscopy (Thermo scientific, ARL Quant'X), which correlated with the transmission electron microscopy (TEM, Tecnai Osiris, FEI) measurements. The chemistries of the Ru substrate and TiO_2 thin films were analyzed via x-ray photoelectron spectroscopy (XPS, VG, Sigma Probe). Glancing angle incident x-ray diffraction (GA-XRD, PANalytical, X'pert Pro) was used to examine the crystal structure of the films with an incident angle of 0.5°. The surface morphology and roughness were observed via atomic force microscopy (AFM, AVT8080, Pucotech), while the electrical properties were evaluated by measuring the capacitance–voltage and the current–voltage using Agilent 4284 and 4156C, respectively.

3. Results and discussion

Firstly, the chemical states of the Ru substrates with respect to the ambient conditions of the pretreatment process were examined via XPS (figure 1). Figures 1(a)–(d) show the Ru 3d XPS spectra (data points) of the pristine Ru substrate ($Ru_{pristine}$) as well as Ru substrates with pretreatment in N_2 (Ru_{-N}), $N_2 + H_2$ (Ru_{-H}), and $N_2 + O_2$ (Ru_{-O}). The same figures also show the deconvoluted spectra (lines) assuming that the Ru 3d peaks are composed of Ru $3d_{5/2}$ peaks centered at the 280.0, 280.8, and 281.8 eV binding energies

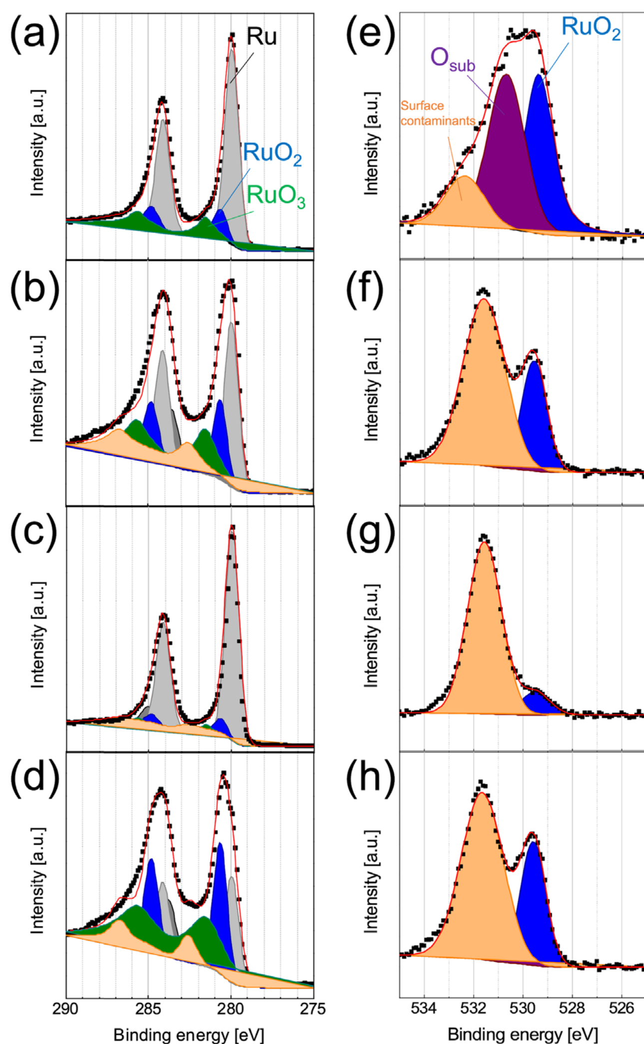

Figure 1. Peak fits of (a)–(d) Ru 3d and (e)–(f) O 1s spectra of (a), (e) $Ru_{pristine}$, (b), (f) Ru_{-N}, (c), (g) Ru_{-H}, and (d), (h) Ru_{-O}. In Ru 3d spectra, left-side peaks are originated from $3d_{3/2}$. Peak deconvolution was conducted with $3d_{5/2}$ spectra (right-side peaks).

(BEs), which correspond to metallic Ru, RuO_2, and RuO_3, respectively [37]. The Ru 3d spectrum of $Ru_{pristine}$ reveals that the latter consists of metal Ru components with a small RuO_2 component contribution, which is reduced by employing the pretreatment under $N_2 + H_2$ ambient conditions (figure 1(c)). Conversely, the RuO_2 contribution is increased when pretreated under N_2 and $N_2 + O_2$ ambient conditions (figures 1(b) and (d)), implying that both pretreatment processes induce the oxidation of the Ru substrate to RuO_2 under N_2 and $N_2 + O_2$ ambient conditions. It should be emphasized that even under the N_2 ambient condition, Ru substrate oxidation can be induced. To clarify this behavior, the O 1s spectra of Ru substrates were examined. The O 1s spectra (figures 1(e)–(h)) were also deconvoluted, wherein the peaks located at the 529.5, 530.7, and ~532 eV BEs corresponded to the oxygen in the bulk RuO_2, the surface-adsorbed or subsurface oxygen (O_{sub}) [45, 46], and surface contamination, such as water or hydrocarbons [47], respectively. Among the Ru substrates, a significant contribution from the peak at 530.7 eV is only observed in the O 1s spectra from $Ru_{pristine}$, thereby indicating that only $Ru_{pristine}$ has a considerable amount of O_{sub}, whose concentration in the substrate is reduced by conducting the pretreatment under any ambient condition. By conducting the pretreatment under the $N_2 + H_2$ ambient condition, O_{sub} would be eliminated by the reduction atmosphere. Conversely, decreasing the peak from O_{sub} in the Ru substrate after conducting Ru_{-O} and Ru_{-N} is also observed, even though these are not reducing atmospheres. Moreover, the Ru 3d and O 1s spectra from Ru_{-O} and Ru_{-N} indicate the formation of RuO_2. Notably, the intensity of the peaks corresponding to RuO_2 in the Ru 3d and O 1s spectra was increased in Ru_{-N} and Ru_{-O} (figure S1 is available online at stacks.iop.org/NANO/32/045201/mmedia in the supplemental material). For Ru_{-O}, the oxidizing atmosphere induces the formation of RuO_2, as shown from the highest RuO_2 peak contribution in the Ru 3d spectrum in figure 1(d), implying that the reduction of the peak from O_{sub} would be caused by the screening effect from the formation of RuO_2 on the surface of the Ru substrate or by decreasing the consumption of O_{sub} during the formation of RuO_2 by the contribution of O_{sub} as an oxygen source. Although N_2 pretreatment does not serve the function of an oxygen source under the ambient condition, the formation of RuO_2 is significantly observed in Ru_{-N}. This indicates that O_{sub} in $Ru_{pristine}$ can contribute to the formation of RuO_2 as an oxygen source, and the amount of O_{sub} in $Ru_{pristine}$ is sufficient to form RuO_2 on the surface, even in an inert atmosphere. Furthermore, the Ru substrates that undergo the pretreatment process have different oxidation levels depending on the difference in the amount of oxygen under each pretreatment ambient condition; all of the pretreatment conditions eliminate available O_{sub}.

The difference in the available O_{sub} strongly affects film growth behavior during subsequent ALD processes. The thickness of the TiO_2 thin film deposited on various Ru substrates via ALD was measured, as shown in figure 2(a). Moreover, figure 2(b) reveals the differentiating growth per cycle (ΔGPC) of the TiO_2 thin film as a function of the number of TiO_2 ALD cycles, which can be acquired from the data in figure 2(a). In the initial TiO_2 deposition stage, ΔGPC is higher than that whereof the substrate is covered with the TiO_2 film. Notably, the ΔGPC values of TiO_2 on the Ru substrates become identical at 0.02 nm/cycle after conducting 50 ALD cycles, wherein the thickness of the deposited TiO_2 is approximately 1.5 nm. However, at up to 50 ALD cycles, the ΔGPC on $Ru_{pristine}$ is relatively higher than that on the pretreated Ru substrates (figure 2(b)), resulting in higher film thicknesses (figure 2(a)). The Ti-precursor-only sequence was performed as an ALD sequence consisting of TTIP feeding and purge of 0.5 and 21 s, respectively. Steady TiO_2 growth under the Ti-precursor-only condition was observed solely on the $Ru_{pristine}$ substrate (figure 2(c)). In the case of employing the pretreated Ru substrate, TiO_2 growth was saturated at a TTIP feeding of 30 cycles. Conversely, the ΔGPC of TiO_2 at 50 cycles on $Ru_{pristine}$ exhibited a comparable value of 0.010 nm/cycle to that at 20 and 30 cycles of 0.017 and 0.020 nm/cycle, respectively (figure 2(d)).

Moreover, the morphology of TiO_2 thin films is strongly influenced by the chemistry of Ru substrates (figures 3, S2,

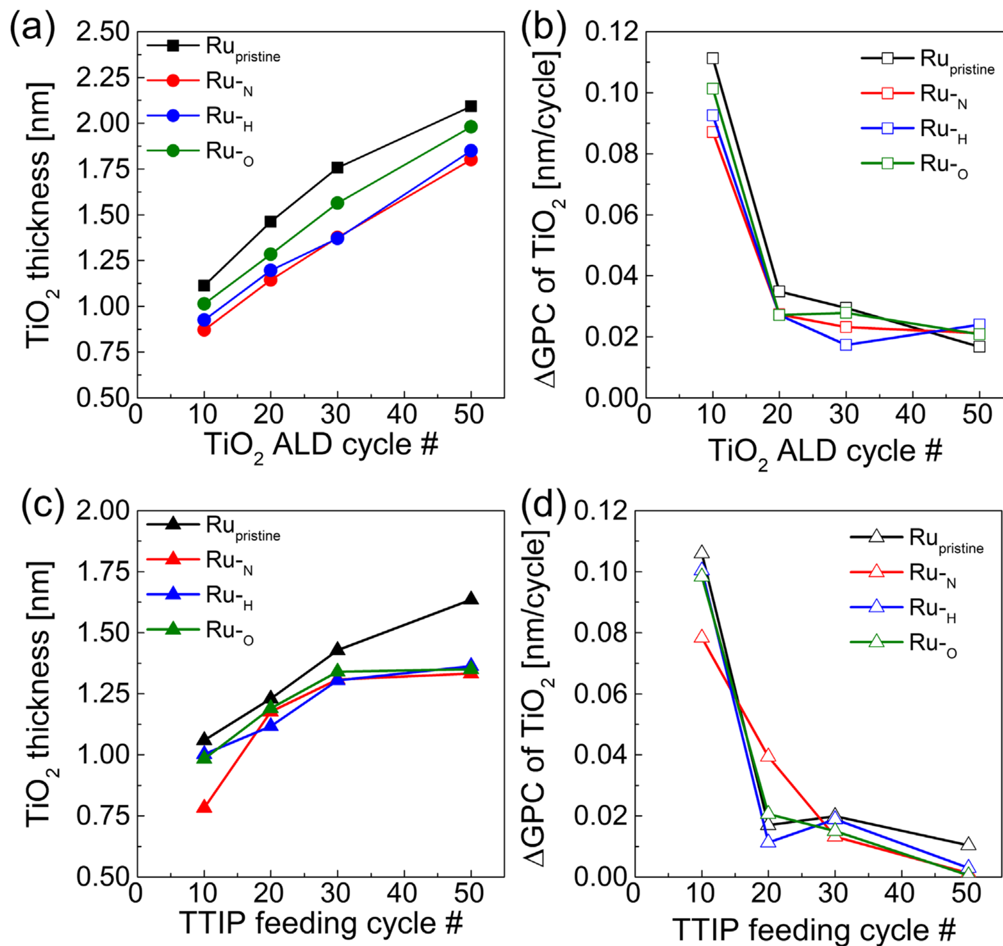

Figure 2. (a), (c) TiO_2 thin film thickness, and (b), (d) differentiating growth rate (ΔGPC) as a function of cycle number of (a), (b) TiO_2 ALD, and (c), (d) Ti-precursor-only feeding sequence.

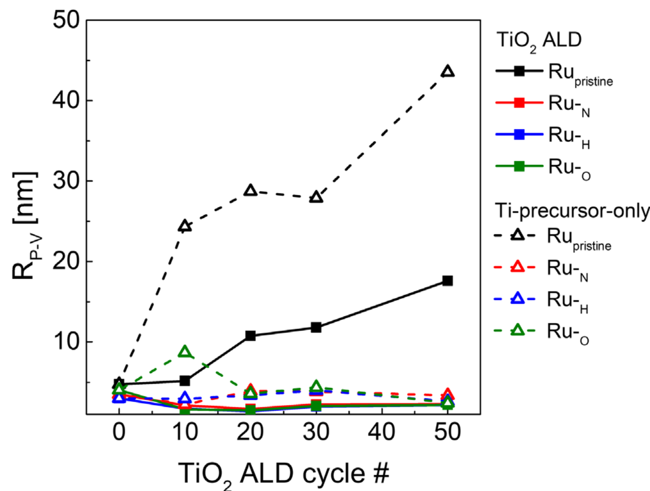

Figure 3. Peak-to-valley roughness (R_{P-V}) of TiO_2 thin film deposited on various Ru substrates as a function of TiO_2 ALD and Ti-precursor-only sequence cycle number.

and table S1). The AFM analyses reveals that the pre-treatment process does not induce morphological degradation (figures S2(a)–(d)). Whereas no morphological degradation was observed in the case of employing pretreated Ru substrates, severe degradation was evident when the TiO_2 thin film was deposited on the $Ru_{pristine}$ substrate (closed square in figures 3 and S2(e)–(h)). This degradation in roughness increases with the TiO_2 ALD cycle number up to 50 cycles, whereby an approximately 2 nm thick TiO_2 thin film is deposited. The observation of distinctive behaviors, higher ΔGPC, and severe morphological degradation in the initial stage only on $Ru_{pristine}$ implies that O_{sub} in Ru plays a key role in the chemical reaction with Ru substrate, TTIP, and O_3 during subsequent TiO_2 ALD processes in the early stage [37]. To comprehensively clarify the chemical reaction during TiO_2 ALD processes, the ΔGPC enhancement and morphological degradation in the initial stage under the conditions of the Ti-precursor-only and O_3-only sequences were examined. In case of the Ti-precursor-only sequence, only the severe morphological degradation was observed in the case of employing the $Ru_{pristine}$ substrate, as well (opened figures 3(c)–(g) and S2(i)–(l)). In the case of performing the Ti-precursor-only sequence, the ΔGPC enhancement and morphological degradation exhibited identical behaviors, as shown in the initial stage of the TiO_2 ALD. Furthermore, the morphological degradation under the O_3-only feeding condition was observed in $Ru_{pristine}$ and Ru-$_H$, but not in Ru-$_O$ and Ru-$_N$ (figures S2(m)–(p)). The substrate was covered with rod-shaped protrusions with heights of ∼100–200 nm in the

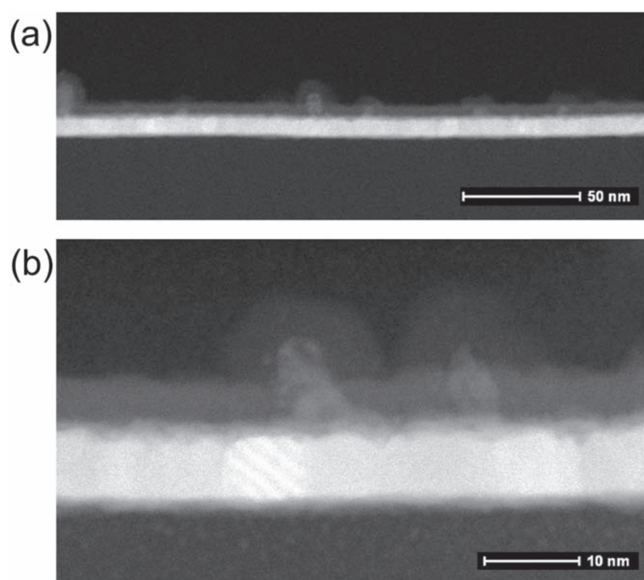

Figure 4. TEM image of an 8 nm thick TiO_2 thin film deposited on the $Ru_{pristine}$ substrate in: (a) a low magnification and (b) a high-resolution mode.

case of $Ru_{pristine}$ and Ru-$_H$. The protrusion was also observed on the Ru-$_N$ and Ru-$_O$ substrates, although its number was significantly lower than that of $Ru_{pristine}$ and Ru-$_H$. The only difference between $Ru_{pristine}$ and Ru-$_H$, and Ru-$_O$ and Ru-$_N$ is that the metallic Ru constituent in the substrate is either dominant or otherwise.

To clarify the origin and formation mechanism of the protrusion, the microstructure of the cross section of the TiO_2-deposited Ru substrate was investigated via TEM. Figure 4 shows that the protrusions are observed on the surface. From the magnified image of the protrusion (figure 4(b)), it is revealed that the protrusion consists of RuO_2 growing from the Ru substrate, and the growth of the protrusion occurs on the grain boundary of the Ru substrate, while the protrusion has a specific growth direction, perpendicular to the surface. This peculiar RuO_2 protrusion growth behavior on the Ru substrate is consistent with previous report on the nanocolumn structure formation of RuO_2 on Ru substrate [44]; the Ru substrate is covered with very thin RuO_x, exhibiting strong RuO_2 nanocolumn anisotropic growth with an abnormal aspect ratio of 1:3, and preferred growth direction of [110], which has the lower energy. In this regard, it is discovered that the abnormal RuO_2 protrusion is formed during the subsequent ALD processes. Furthermore, the occurrence of the growth at the grain boundary, whereat the O_{sub} concentration is higher than that in the other regions, implies that O_{sub} is the oxygen source for the formation of the RuO_2 protrusion in this result. This well coincides with the above-mentioned results. The protrusion was not observed on the pretreated Ru substrates because of the decreased O_{sub}, as shown in the XPS spectra. In the case of conducting the O_3-only sequence, since only the metallic Ru can incorporate O_{sub} from the O radical during O_3 pulse, only the $Ru_{pristine}$ and Ru-$_H$ substrates exhibited severe protrusion formation. Moreover, the height of the protrusion in the Ti-precursor-only sequence significantly increases to >40 nm at 50 cycles compared to that of the TiO_2 ALD of ∼18 nm at 50 cycles, thereby indicating that an insufficient oxidation atmosphere might facilitate protrusion growth.

From the results shown in above, the protrusion formation during the TiO_2 ALD process from the low oxidation–reduction resistance of the Ru substrate would be explained through the following mechanism: During a subsequent process on the Ru substrate, O_{sub} incorporated in the Ru substrate could form an oxygen-rich RuO_x ($2 < x < 3$) phase, followed by the formation of a stable RuO_2 thin film. However, under a specific low-temperature condition of under 275 °C or short oxidation duration, stoichiometric RuO_2 thin film formation is hindered, thereby resulting in the 3D columnar growth of RuO_x. This condition is consistent with the TiO_2 ALD condition, with a process temperature of 250 °C and oxygen consumption by the chemisorbed TTIP precursor. In other words, the condition whereby O_{sub} dominantly contributes to the oxidation reaction is that which can induce protrusion formation, i.e. the 3D columnar growth of RuO_x. In this regard, the formation of protrusions during the TiO_2 ALD is observed in $Ru_{pristine}$, which only has sufficient O_{sub}. Additionally, the formation of protrusions becomes severe in the case of the Ti-precursor-only sequence, because the contribution of O_{sub} is increased in this case. Moreover, the protrusion formation in the O_3-only sequence would also be caused by the O_{sub} contribution because the severe protrusion formation was observed in $Ru_{pristine}$ and Ru-$_H$, wherein the substrates consisted of metallic Ru. Indeed, all the Ru substrates, regardless of their pretreatment conditions, exhibit morphological degradation covered with columnar RuO_x after conducting the O_3-only sequence (figures S2(m)–(p)). Even in Ru-$_O$ and Ru-$_N$, which have RuO_2 components in the substrate, severe morphological degradation by protrusion formation was observed.

This indicates that the morphological degradation of the Ru-based substrate, Ru or RuO_2, can occur under any circumstance regardless of the reducing or oxidizing atmosphere owing to its weak redox resistance property, thereby limiting the employment of Ru-based thin films as electrodes in various devices. Notably, the ability of the reducing atmosphere to also induce protrusion formation results in the morphological degradation of the Ru substrate in most of metal oxide ALD processes, wherein, a metal precursor is initially introduced on the substrate, and subsequently, the chemisorbed precursor induces a driving force of substrate reduction due to the formation energy of metal oxides. In contrast to the other substrates, Ru has an abundant amount of oxygen in its lattice as O_{sub} [45] and relatively small formation energy of RuO_2 than that of most of metal oxides, thereby resulting in a vigorous reaction of the chemisorbed precursor and oxygen from the substrate. Therefore, it is strongly postulated that the morphological degradation during subsequent TiO_2 ALD processes is related to an O_{sub} reaction in the reducing atmosphere by chemisorbed TTIP. The Ru substrate without any treatment ($Ru_{pristine}$) has a polycrystalline structure, and O_{sub} is present at a certain region right beneath the Ru grain surface. Where TTIP is chemisorbed on the Ru substrate

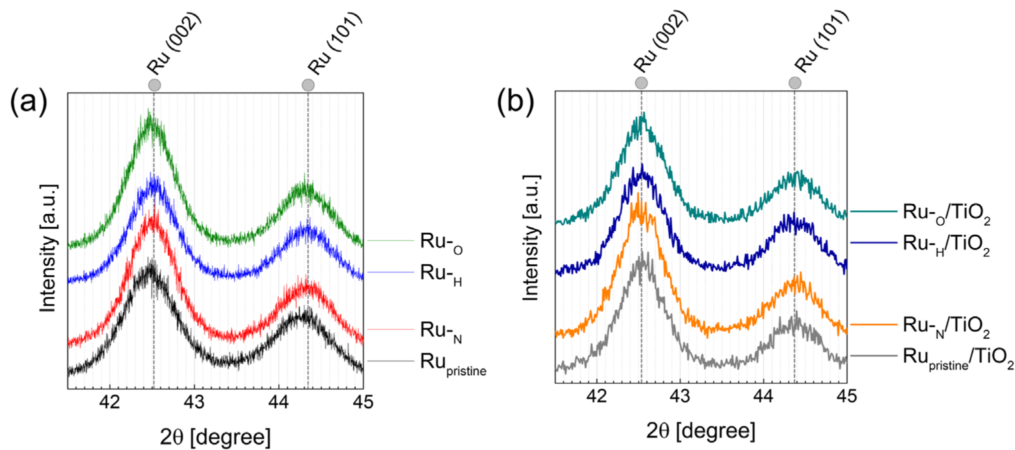

Figure 5. XRD patterns of (a) Ru substrates, and (b) 10 nm thick TiO_2/Ru stacks.

surface, O_{sub} is extracted from the Ru grain to react with chemisorbed TTIP, which induces GPC enhancement in the initial stage of the TiO_2 ALD process. This result corroborates the near-identical morphological degradation behavior observed in both of the Ti-precursor-only and TiO_2 ALD processes. Consequently, it is revealed that the oxygen source feeding step in the ALD sequence does not significantly affect the formation of columnar RuO_x growth.

In this regard, suppressing RuO_x formation by adjusting the ALD process condition would be ineffective. As mentioned above, RuO_x formation is governed by process temperature and O_{sub} concentration. Between them, a higher process temperature is preferable to prevent RuO_x formation; however, it is difficult to change within a specific ALD process, which is governed by the chemistry of the Ti precursor. Furthermore, increasing the process temperature would induce the thermal decomposition of the precursor or chemical vapor deposition-like reaction with chemisorbed precursor and O_{sub}. Accordingly, eliminating O_{sub} would be the most effective way to hinder RuO_x formation. Notably, the O_{sub} concentration was dramatically decreased after conducting pretreatment, as confirmed by XPS analysis (figure 1); thus, inducing the suppression of the RuO_x formation successfully. Moreover, a d-spacing of the Ru lattice from XRD analysis (figure 5) also indicates the change in O_{sub} in the Ru substrates [37] with respect to the pretreatment ambient condition. O_{sub} in Ru expands the Ru lattice, thereby causing a decrease in the 2θ value of the peak corresponding to the Ru lattice. As shown in figure 5(a), $Ru_{\text{-N}}$ and $Ru_{\text{-H}}$ substrates exhibit relatively higher 2θ than that of $Ru_{pristine}$, i.e. they have relatively lower d-spacing, indicating the elimination of the O_{sub} in the pretreated Ru substrates. Consequently, the severe protrusion formation by conducting TiO_2 ALD and the Ti-precursor-only feeding process was not observed in the pretreated Ru substrates. However, eliminating O_{sub} does not guarantee the suppression of protrusion formation. In the case of the O_3-only feeding, severe protrusion formation was observed on $Ru_{pristine}$ as well as on $Ru_{\text{-H}}$. This denotes that the re-incorporation of O_{sub} into the Ru substrate should also be suppressed to avoid the contribution of RuO_x formation by O_{sub}. Notably, the d-spacing values

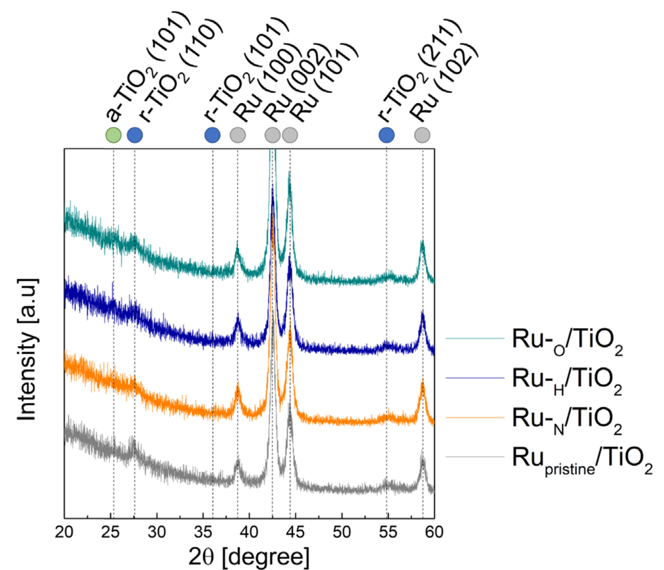

Figure 6. XRD patterns of 20 nm thick TiO_2 thin films deposited on various Ru substrates.

from all the Ru substrates became identical to a 2θ of 42.5° after conducting the deposition process of TiO_2 of 10 nm, meaning that O_{sub} participated as an oxygen source on the subsequent TiO_2 thin film deposition process via ALD.

Furthermore, the characteristics of the Ru substrates as the electrode for TiO_2 thin film have been evaluated. As the electrode for the TiO_2 thin film, demonstrating the rutile crystal structure of TiO_2 by the epitaxial growth behavior with the help of RuO_2 formation is required. To confirm the crystal structure of the TiO_2 thin film deposited on the Ru substrates, XRD analysis was conducted. As shown in figure 6, it is confirmed that the TiO_2 thin film deposited on the Ru substrates was well crystallized to the rutile phase without any contribution from the anatase phase. This result indicates that the RuO_2 layer to induce the rutile crystal structure of deposited TiO_2 is sufficiently formed regardless of the chemical state of the Ru substrates. Notably, the $Ru_{\text{-H}}$ substrate also achieves the formation of the rutile phase, implying that RuO_2 can be formed during the subsequent oxide ALD process even though the substrate does not have

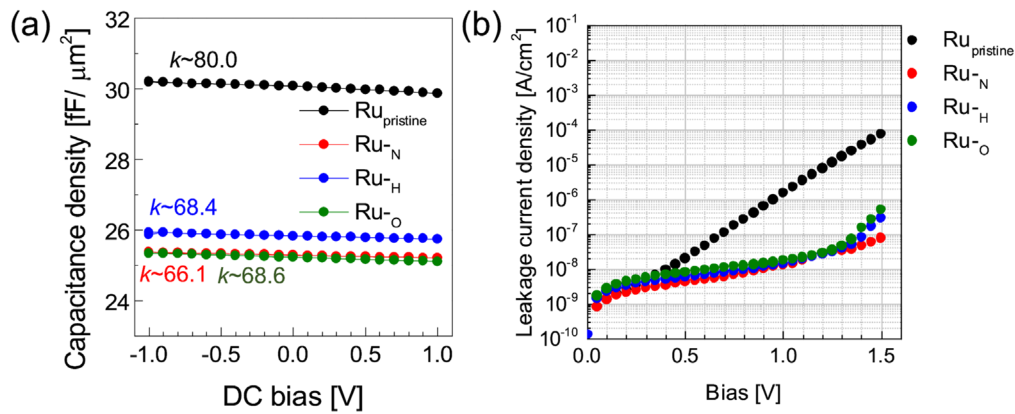

Figure 7. (a) C–V and (b) J–V curves of the MIM capacitor consisting of a 24 nm thick TiO_2 with various Ru substrates.

O_{sub} [35]. Furthermore, the electrical property of the MIM capacitor, which consisted of the Ru substrate and TiO_2 as the bottom electrode and insulator, respectively, was evaluated. Figure 7 shows the capacitance density versus dc bias (C–V) and leakage current density versus applied bias (J–V) curves of the MIM capacitor, which consists of 24 nm thick TiO_2 with various Ru substrates. From the C–V measurement, the TiO_2 thin films deposited on all the Ru substrates exhibited consistency in their k value with rutile-phased TiO_2. However, the TiO_2 on $Ru_{pristine}$ has a higher value of $\sim$80 than that from the pretreated Ru substrates of $\sim$68. This implies that O_{sub} might contribute to the formation of RuO_2, thereby subsequently enhancing the crystallinity of the deposited TiO_2 thin film to the rutile phase. The leakage current density level is significantly reduced to approximately two orders of magnitude from the $Ru_{pristine}$ of 1.47×10^{-6} to $Ru\text{-}_N$, $Ru\text{-}_H$, and $Ru\text{-}_O$ of 1.32×10^{-8}, 1.47×10^{-8}, $1.74 \times 10^{-8}\ A \cdot cm^{-2}$, respectively, at an applied bias of 1.0 V. This leakage current value difference is consistent with the morphology of the TiO_2 thin film. Figure S3 shows the AFM image of a 20 nm thick TiO_2 thin film on various Ru substrates. In the case of $Ru_{pristine}$, severe protrusion formation is observed during the TiO_2 ALD process, as shown in high root mean square roughness (R_q) and peak-to-valley roughness ($R_{P\text{-}V}$) values of 1.423 and 14.3 nm, respectively. Conversely, the pretreated Ru substrates exhibited ameliorated roughness, especially in the case of $Ru\text{-}_H$, R_q and $R_{P\text{-}V}$ were reduced to 0.7944 and 6.30 nm, respectively. The XPS analysis shows that the $Ru\text{-}_O$ and $Ru\text{-}_N$ substrates are a mixture of Ru and RuO_2, which is unfavorable for use as the bottom electrode because of the vigorous redox reaction would occur during the ALD process owing to the catalytic effect of Ru on the reduction of RuO_2 [43]. For the $Ru\text{-}_H$ substrate, the leakage current density is sufficiently low, which implies that any Ru substrate degradation during the TiO_2 ALD process is induced. Consequently, pretreatment effectively reduces the leakage current density by enhancing morphology, as well as relatively induces less crystallization by suppressing RuO_2 formation.

Finally, the leakage current density versus equivalent oxide thickness (J–t_{ox}) curve for the TiO_2 thin film with varied thicknesses of 10–20 nm deposited on $Ru_{pristine}$ and $Ru\text{-}_H$ were evaluated (figure 8). As confirmed in previous results, the TiO_2 thin film deposited on the $Ru\text{-}_H$ substrate exhibited a relatively reduced capacitance density compared with the $Ru_{pristine}$ substrate (figure S4(a)). However, the capacitance density of the TiO_2 thin film on the $Ru\text{-}_H$ substrate exhibited a higher value than that of $Ru_{pristine}$ in the case of the 10 nm thick TiO_2 thin film. This is because a too leaky TiO_2 thin film on $Ru_{pristine}$ degrades capacitance measurement. Notably, the dielectric loss exhibited an excessively high value of >0.1. Moreover, the leakage current density value was also too high, as shown in figure S4(b). For the leakage current density, the TiO_2 thin films deposited on $Ru_{pristine}$ exhibited a higher value than those deposited on $Ru\text{-}_H$. Moreover, as the thickness of the TiO_2 thin film decreased, the deterioration in the leakage current density of TiO_2 on $Ru_{pristine}$ became worse than that on $Ru\text{-}_H$. Eventually, even though the TiO_2 thin film on $Ru_{pristine}$ had a relatively higher k value, the effective t_{ox} scaling of the TiO_2 thin film was achieved with the $Ru\text{-}_H$ substrate owing to the leakage current density reduction.

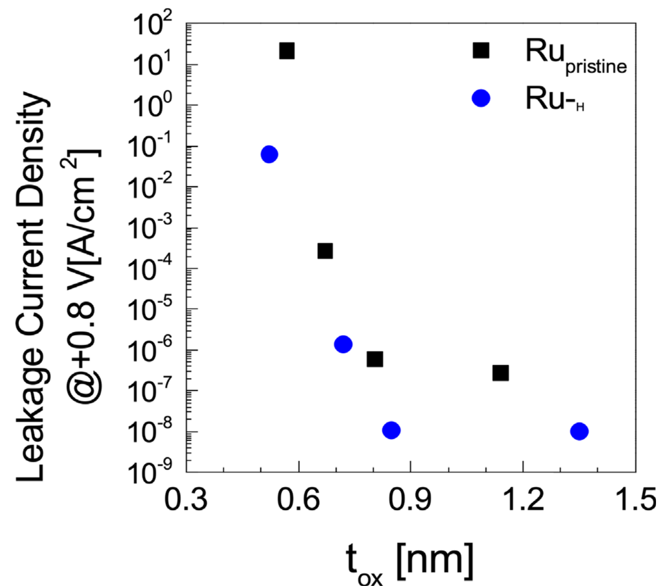

Figure 8. J–t_{ox} plot of the MIM capacitor with various thicknesses of TiO_2 thin films deposited on the $Ru_{pristine}$ and $Ru\text{-}_H$ substrates.

4. Conclusion

We investigated the change in the chemistry of the Ru electrode due to the subsequent processes to suppress protrusion formation, which occurred in the as-deposited Ru electrode that had a sufficient O_{sub} concentration during the TiO_2 ALD process. The O_{sub} incorporation into the Ru substrate was affected by the ambient conditions of the pretreatment process. It was revealed from the experiments using the Ti-precursor-only and O_3-only feeding sequences that repeating the redox reaction by precursor and oxygen source feeding in the subsequent ALD process causes protrusion formation. The TEM results revealed that the protrusion consisted of RuO_2 achieved from the reaction of Ru and O_{sub}. In this regard, the pretreatment under the $N_2 + H_2$ ambient condition led to successful suppression of protrusion formation. This imparts higher electrical properties on TiO_2 deposited on the pretreated Ru electrode. Therefore, it is established that eliminating O_{sub} from Ru is the most effective way to apply the Ru substrate in practical electronic devices.

Acknowledgments

This work was supported by the Technology Innovation Program (No. 20003555) funded by the Ministry of Trade, Industry & Energy (MOTIE, Korea) and the National Research Foundation of Korea (NRF) grant funded by the Korea government (MSIT) (No. 2018R1C1B5045854). W Jeon also acknowledges financial support by Samsung Advanced Institute of Technology, and Kyung Hee University in 2020 (No. KHU-20201107).

ORCID iDs

Woojin Jeon https://orcid.org/0000-0002-8477-9124

References

[1] Yoon K J *et al* 2017 Double-layer-stacked one diode-one resistive switching memory crossbar array with an extremely high rectification ratio of 10 9 *Adv. Electron. Mater.* **3** 1700152

[2] Govoreanu B, Adelmann C, Redolfi A, Zhang L, Clima S and Jurczak M 2014 High-performance metal–insulator–metal tunnel diode selectors *IEEE Electron Device Lett.* **35** 63–5

[3] Gonon P, Mougenot M, Vallée C, Jorel C, Jousseaume V, Grampeix H and El Kamel F 2010 Resistance switching in HfO_2 metal–insulator–metal devices *J. Appl. Phys.* **107** 074507

[4] Lee D-Y, Tsai T-L and Tseng T-Y 2013 Unipolar resistive switching behavior in $Pt/HfO_2/TiN$ device with inserting ZrO_2 layer and its 1 diode-1 resistor characteristics *Appl. Phys. Lett.* **103** 032905

[5] Lee W, Han J H, Jeon W, Yoo Y W, Lee S W, Kim S K, Ko C-H, Lansalot-Matras C and Hwang C S 2013 Atomic layer deposition of $SrTiO_3$ films with cyclopentadienyl-based precursors for metal–insulator–metal capacitors *Chem. Mater.* **25** 953–61

[6] Park W Y, Kim G H, Seok J Y, Kim K M, Song S J, Lee M H and Hwang C S 2010 A $Pt/TiO_2/Ti$ Schottky-type selection diode for alleviating the sneak current in resistance switching memory arrays *Nanotechnology* **21** 195201

[7] Jeon W, Kim Y, An C H, Hwang C S, Gonon P and Vallee C 2018 Demonstrating the ultrathin metal–insulator–metal diode using TiN/ZrO_2–Al_2O_3–ZrO_2 Stack by employing RuO_2 top electrode *IEEE Trans. Electron Devices* **65** 660–6

[8] Jeon W, Salicio O, Chaker A, Gonon P and Vallee C 2019 Controlling the current conduction asymmetry of HfO_2 metal–insulator–metal diodes by interposing Al_2O_3 layer *IEEE Trans. Electron Devices* **66** 402–6

[9] Mueller W *et al* 2005 Challenges for the DRAM cell scaling to 40 nm *Tech. Dig.—Int. Electron Devices Meet. IEDM* 2005, 336–9

[10] Chaker A, Gonon P, Vallée C and Bsiesy A 2017 High capacitance density of 185 nF mm^{-2} achieved in three-dimensional MIM structures using TiO_2 as a dielectric *Appl. Phys. Lett.* **110** 1–5

[11] Fazan P C 1994 Trends in the development of ulsi dram capacitors *Integr. Ferroelectr.* **4** 247–56

[12] Kotecki D E 1997 A review of high dielectric materials for dram capacitors *Integr. Ferroelectr.* **16** 1–19

[13] Scott J F 1998 High-dielectric constant thin films for dynamic random access memories (DRAM) *Annu. Rev. Mater. Sci.* **28** 79–100

[14] Kim S K and Popovici M 2018 Future of dynamic random-access memory as main memory *MRS Bull.* **43** 334–9

[15] Wilk G D, Wallace R M and Anthony J M 2001 High-κ gate dielectrics: current status and materials properties considerations *J. Appl. Phys.* **89** 5243–75

[16] Robertson J and Wallace R M 2015 High-K materials and metal gates for CMOS applications *Mater. Sci. Eng. R* **88** 1–41

[17] Jeon W 2019 Recent advances in the understanding of high- k dielectric materials deposited by atomic layer deposition for dynamic random-access memory capacitor applications *J. Mater. Res.* **35** 1–20

[18] Cho H J *et al* 2007 New TIT capacitor with $ZrO_2/Al_2O_3/ZrO_2$ dielectrics for 60 nm and below DRAMs *Solid State Electron.* **51** 1529–33

[19] Cho H *et al* 2006 New TIT capacitor with $ZrO_2/Al_2O_3/ZrO_2$ dielectrics for 60 nm and below DRAMs *2006 European Solid-State Device Research Conf.* (Piscataway, NJ: IEEE) 146–9

[20] Kil D-S *et al* 2006 Development of new $TiN/ZrO_2/Al_2O_3/ZrO_2/TiN$ capacitors extendable to 45 nm generation DRAMs replacing HfO_2 based dielectrics *2006 Symp. on VLSI Technology, 2006. Digest of Technical Papers* (Piscataway, NJ: IEEE) 38–9

[21] Jeon W, Chung H-S, Joo D and Kang S-W 2008 $TiO_2/Al_2O_3/TiO_2$ nanolaminated thin films for DRAM capacitor deposited by plasma-enhanced atomic layer deposition *Electrochem. Solid-State Lett.* **11** H19

[22] Kim S K, Choi G-J, Lee S Y, Seo M, Lee S W, Han J H, Ahn H-S, Han S and Hwang C S 2008 Al-doped TiO_2 films with ultralow leakage currents for next generation DRAM capacitors *Adv. Mater.* **20** 1429–35

[23] Jeon W, Rha S H, Lee W, Yoo Y W, An C H, Jung K H, Kim S K and Hwang C S 2014 Controlling the Al-doping profile and accompanying electrical properties of rutile-phased TiO_2 thin films *ACS Appl. Mater. Interfaces* **6** 7910–7

[24] Jeon W, Yoo S, Kim H K, Lee W, An C H, Chung M J, Cho C J, Kim S K and Hwang C S 2014 Evaluating the top electrode material for achieving an equivalent oxide

thickness smaller than 0.4 nm from an Al-doped TiO_2 film *ACS Appl. Mater. Interfaces* **6** 21632–7

[25] Jeon W, Rha S H, Lee W, An C H, Chung M J, Kim S H, Cho C J, Kim S K and Hwang C S 2015 Asymmetry in electrical properties of Al-doped TiO_2 film with respect to bias voltage *Phys. Status Solidi—Rapid Res. Lett.* **9** 410–3

[26] Shim J H, Choi H J, Kim Y, Torgersen J, An J, Lee M H and Prinz F B 2017 Process-property relationship in high-: K ALD $SrTiO_3$ and $BaTiO_3$: a review *J. Mater. Chem.* C **5** 8000–13

[27] Swerts J *et al* 2014 Leakage control in 0.4 nm EOT $Ru/SrTiO_x/Ru$ metal–insulator–metal capacitors: process implications *IEEE Electron Device Lett.* **35** 753–5

[28] Lee W *et al* 2015 Improved initial growth behavior of SrO and $SrTiO_3$ films grown by atomic layer deposition using $\{Sr(demamp)(tmhd)\}_2$ as Sr-precursor *Chem. Mater.* **27** 3881–91

[29] Lee W, Han J H, Lee S W, Han S, Jeon W J and Hwang C S 2012 Controlling the initial growth behavior of $SrTiO_3$ films by interposing Al_2O_3 layers between the film and the Ru substrate *J. Mater. Chem.* **22** 15037–44

[30] Chung M J, Jeon W, An C H, Kim S H, Lee Y K, Lee W and Hwang C S 2018 Quantitative analysis of the incorporation behaviors of Sr and Ti atoms during the atomic layer deposition of $SrTiO_3$ thin films *ACS Appl. Mater. Interfaces* **10** 8836–44

[31] Mojarad S A, Kwa K S K, Goss J P, Zhou Z, Ponon N K, Appleby D J R, Al-Hamadany R A S and O'Neill A 2012 A comprehensive study on the leakage current mechanisms of $Pt/SrTiO_3/Pt$ capacitor *J. Appl. Phys.* **111** 014503

[32] Lee D-K, Kwon S-H and Ahn J-H 2019 Growth of rutile-TiO_2 thin films via Sn doping and insertion of ultra-thin SnO_2 interlayer by atomic layer deposition *Mater. Lett.* **246** 1–4

[33] Niemelä J P, Marin G and Karppinen M 2017 Titanium dioxide thin films by atomic layer deposition: a review *Semicond. Sci. Technol.* **32** 093005

[34] An C H *et al* 2019 Controlling the electrical characteristics of $ZrO_2/Al_2O_3/ZrO_2$ capacitors by adopting a Ru top electrode grown via atomic layer deposition *Phys. Status Solidi—Rapid Res. Lett.* **13** 1800454

[35] Kim S K, Kim W D, Kim K M, Hwang C S and Jeong J 2004 High dielectric constant TiO_2 thin films on a Ru electrode grown at 250 °C by atomic-layer deposition *Appl. Phys. Lett.* **85** 4112–4

[36] Han J H, Han S, Lee W, Lee S W, Kim S K, Gatineau J, Dussarrat C and Hwang C S 2011 Improvement in the leakage current characteristic of metal–insulator–metal capacitor by adopting RuO_2 film as bottom electrode *Appl. Phys. Lett.* **99** 022901

[37] Jeon W, Lee W, Yoo Y W, An C H, Han J H, Kim S K and Hwang C S 2014 Chemistry of active oxygen in RuO_x and its influence on the atomic layer deposition of TiO_2 films *J. Mater. Chem.* C **2** 9993–10001

[38] Kim J-Y, Kil D-S, Kim J-H, Kwon S-H, Ahn J-H, Roh J-S and Park S-K 2012 Ru films from Bis(ethylcyclopentadienyl) ruthenium using ozone as a reactant by atomic layer deposition for capacitor electrodes *J. Electrochem. Soc.* **159** H560–4

[39] Yeo S, Park J Y, Lee S J, Lee D J, Seo J H and Kim S H 2015 Ruthenium and ruthenium dioxide thin films deposited by atomic layer deposition using a novel zero-valent metalorganic precursor, (ethylbenzene)(1,3-butadiene)Ru (0), and molecular oxygen *Microelectron. Eng.* **137** 16–22

[40] Kim J H, Kil D S, Yeom S J, Roh J S, Kwak N J and Kim J W 2007 Modified atomic layer deposition of RuO_2 thin films for capacitor electrodes *Appl. Phys. Lett.* **91** 5–8

[41] Han J H, Lee S W, Choi G J, Lee S Y, Hwang C S, Dussarrat C and Gatineau J 2009 Chemical vapor deposition of Ru thin films with an enhanced morphology, thermal stability, and electrical properties using a RuO_4 precursor *Chem. Mater.* **21** 207–9

[42] Han J H, Lee S W, Choi G J, Lee S Y, Hwang C S, Dussarrat C and Gatineau J 2019 Pulsed-chemical vapor deposition of ruthenium and ruthenium dioxide thin films using RuO_4 precursor for the DRAM capacitor electrode *ECS Trans.* **19** 717–28

[43] Han J H, Lee S W, Kim S K, Han S, Hwang C S, Dussarrat C and Gatineau J 2010 Growth of RuO_2 thin films by pulsed-chemical vapor deposition using RuO_4 precursor and 5% H_2 reduction gas *Chem. Mater.* **22** 5700–6

[44] Coloma Ribera R, Van De Kruijs R W E, Kokke S, Zoethout E, Yakshin A E and Bijkerk F 2014 Surface and sub-surface thermal oxidation of thin ruthenium films *Appl. Phys. Lett.* **105** 131601

[45] Todorova M, Li W X, Ganduglia-Pirovano M V, Stampfl C, Reuter K and Scheffler M 2002 Role of subsurface oxygen in oxide formation at transition metal surfaces *Phys. Rev. Lett.* **89** 1–4

[46] Dey S K, Goswami J, Gu D, De Waard H, Marcus S and Werkhoven C 2004 Ruthenium films by digital chemical vapor deposition: selectivity, nanostructure, and work function *Appl. Phys. Lett.* **84** 1606–8

[47] Hudec B *et al* 2013 Impact of plasma treatment on electrical properties of TiO_2/RuO_2 based DRAM capacitor *J. Phys. D: Appl. Phys.* **46** 385304